Ulster
University

Improved pharmacokinetic and lymphatic uptake of Rose Bengal after transfersome intradermal deposition using hollow microneedles

Demartis, S., Rassu, G., Anjani, Q. K., Volpe-Zanutto, F., Hutton, A., Sabri, A. H. B., McCarthy, H., Giunchedi, P., Donnelly, R. F., & Gavini, E. (2024). Improved pharmacokinetic and lymphatic uptake of Rose Bengal after transfersome intradermal deposition using hollow microneedles. *Journal of Controlled Release*, *369*, 363-375. https://doi.org/10.1016/j.jconrel.2024.03.048

Link to publication record in Ulster University Research Portal

Document Version
Publisher's PDF, also known as Version of record

Improved pharmacokinetic and lymphatic uptake of Rose Bengal after transfersome intradermal deposition using hollow microneedles

Sara Demartis [a], Giovanna Rassu [b,*], Qonita Kurnia Anjani [c], Fabiana Volpe-Zanutto [c], Aaron R.J. Hutton [c], Akmal B. Sabri [c], Helen O. McCarthy [c], Paolo Giunchedi [b], Ryan F. Donnelly [c,*], Elisabetta Gavini [b]

[a] Department of Chemical, Mathematical, Natural and Physical Sciences, University of Sassari, Sassari 07100, Italy
[b] Department of Medicine and Surgery, University of Sassari, Sassari 07100, Italy
[c] School of Pharmacy, Queen's University, Belfast 97 Lisburn Road, Belfast BT9 7BL, United Kingdom

ARTICLE INFO

ABSTRACT

The lymphatic system is active in several processes that regulate human diseases, among which cancer progression stands out. Thus, various drug delivery systems have been investigated to promote lymphatic drug targeting for cancer therapy; mainly, nanosized particles in the 10–150 nm range quickly achieve lymphatic vessels after an interstitial administration. Herein, a strategy to boost the lymphotropic delivery of Rose Bengal (RB), a hydrosoluble chemotherapeutic, is proposed, and it is based on the loading into Transfersomes (RBTF) and their intradermal deposition *in vivo* by microneedles. RBTF of 96.27 ± 13.96 nm (PDI = 0.29 ± 0.02) were prepared by a green reverse-phase evaporation technique, and they showed an RB encapsulation efficiency of $98.54 \pm 0.09\%$. *In vitro*, RBTF remained physically stable under physiological conditions and avoided the release of RB. *In vivo*, intravenous injection of RBTF prolonged RB half-life of 50 min in healthy rats compared to RB intravenous injection; the RB half-life in rat body was further increased after intradermal injection reaching 24 h, regardless of the formulation used. Regarding lymphatic targeting, RBTF administered intravenously provided an RB accumulation in the lymph nodes of 12.3 ± 0.14 ng/mL after 2 h, whereas no RB accumulation was observed after RB intravenous injection. Intradermally administered RBTF resulted in the highest RB amount detected in lymph nodes after 2 h from the injection (84.2 ± 25.10 ng/mL), which was even visible to the naked eye based on the pink colouration of the drug. In the case of intradermally administered RB, RB in lymph node was detected only at 24 h (13.3 ± 1.41 ng/mL). In conclusion, RBTF proved an efficient carrier for RB delivery, enhancing its pharmacokinetics and promoting lymph-targeted delivery. Thus, RBTF represents a promising nanomedicine product for potentially facing the medical need for novel strategies for cancer therapy.

1. Introduction

The lymphatic vasculature is active in various functional processes that maintain human health. Deep investigations on the lymphatic vasculature in pathophysiological conditions have created opportunities for developing novel therapeutics and medical strategies to eradicate certain diseases. [1]. In these regards, the importance of lymphatics in cancer staging and prognosis has been documented for myriad cancer types, with higher emphasis on melanoma and carcinoma of the breast, endometrium, colon, lung, prostate, ovary, pancreas and in the head and neck [2,3]. Frequently, metastases arise from the dissemination of malignant cells through lymphatic vasculature that finally arrives at the lymph nodes, whose role should be cancer containment consequent to their ability to act as a filter for pathogenic particles [1]. Nevertheless, sometimes lymph nodes fail in this role, and malignant cells leave *via* the efferent lymphatic vessel, forming distant metastases [4,5]. Traditionally, a combination of surgery, chemotherapy and radiotherapy has been employed to eradicate cancer metastases; still, two pieces of evidence need to be considered: (a) metastases account for >90% of cancer-related deaths and to date, they remain essentially untreatable; (b) surgery, chemotherapy and radiotherapy are not exempt from serious disadvantages. Many complications arise after surgery; also, microscopic lesions may persist after mass removal, requiring additional treatment, such as radiotherapy, commonly reporting long-term toxicity

and limited efficacy [6–9]. Chemotherapy often results in unspecific drug delivery and difficulty achieving the appropriate drug dosage to the tumour site, consequent to a narrow therapeutic window of drugs or the poor biopharmaceutical profile [10,11]. This evidence, in combination with the role ascribed to the lymphatics in malignancy progression, makes this system highly attractive for novel research on cancer therapy [12].

Different lymphatic-targeting strategies have been tested to determine the most favourable administration route, the influence of the drug's molecular weight, and the eventual use of a drug carrier [13–15]. It is now clear that after an interstitial administration (*e.g.* intradermal, intramuscular, subcutaneous), molecules move through the interstitium and enter the lymphatics *via* the interendothelial tight junctions driven by the fluid flow. It was observed that the intradermal injection could lead to a localised increase in interstitial pressure within the dermis, increasing the rate of drug drainage into the lymphatics compared to the intramuscular or subcutaneous injection [16,17]. The relatively high hydrodynamic pressure and the highly developed lymphatic vasculature of the skin make the cutaneous and percutaneous routes ideal for lymphatic targeting. Additionally, nanosized drug carriers (NCs) revealed success for the lymph-targeted delivery of therapeutics since lymphatic capillaries are size-dependent permeable [12,18,19]. NCs below 150 nm were observed to enter lymph vessels once deposited into the skin; notably, NCs in the range of 10–100 nm are taken up effectively by the lymphatics, whereas NCs > 100 nm are absorbed slowly or are retained at the administration site. Lastly, NPs < 10 nm preferentially enter blood capillaries [18,20–22].

Among NCs employed for drug delivery through the skin, transfersomes (TFs) are the most innovative and efficient carriers. Designed to overcome the rigid structure of their ancestor, the liposomes, TFs are formulated with the additional presence of surfactants (edge activators, EAs), which increases the lipid bilayer fluidity, leading to ultra-deformability. EAs tend to accumulate at the site of high stress due to their propensity for significantly curved structures and reduce the energy costs required for deformation. This way, TFs can pass through the tight migration pathway of the skin tissue, minimising undesired breakage and drug loss [23–26]. Therefore, TFs may successfully reach lymphatic capillaries intact following intradermal deposition, representing a valid lymphotropic delivery system. Nevertheless, little is found in the literature in this regard. Notably, articles investigating lymphatic targeting using TFs primarily focused on tumour metastases therapy [27–29] or immunotherapy [30,31] frequently in association with the microneedle (MN) technique. MNs are the new generation of (trans)dermal patches and comprise many thin and microscopic projections (400–900 μm length) that painlessly pierce the skin to deposit the drug in the intradermal space, avoiding the undesired loss at the skin surface. This way, MNs may substitute the old-standing intradermal injection, and different types have been developed to date, including hollow, polymer dissolving, hydrogel-forming and coated MNs [13,32–37].

Based on these premises, we previously described the development and characterisation of a TF dispersion, loading the chemotherapeutic Rose Bengal (RB), that was subsequently included in a polymer dissolving-type MN array to favour the intradermal deposition of RB-loaded TF (RBTF) [38,39]. RB is a dianionic purplish dye of xanthene structure with photosensitising properties exhibiting intrinsic toxicity for malignant cells [40]. RB anticancer properties have been widely investigated and established on multiple cancer cell lines, including skin, breast, ovarian and colon cancers [41–43]. Currently, RB is undergoing clinical trials for metastatic melanoma therapy with the name of PV-10® (Provectus Biopharmaceuticals, INC), and it was designated as an Orphan Drug by the Food and Drug Administration (FDA) to treat metastatic melanoma, neuroblastoma, and hepatocellular carcinoma. Clinical trials revealed that RB is characterised by a dual mechanism of action, selective for malignant cells. As soon as it is administered, RB stimulates the ablation on lesions directly treated due to lysozyme-induced and apoptotic cell death. Subsequently, RB triggers a specific tumour immune response with activity on distant non-treated or bystander lesions [41,44]. Despite its remarkable potential as a chemotherapeutic, RB translation to clinics is hampered by its chemical-physical profile. The principal limits of RB are high water solubility (100 g/L), which causes a half-life of 30 mins, and poor permeability, as defined by its logP of 0.59, which obliges multiple excruciating intra-tumoral injections to reach the therapeutic dose [40,41,45]. Also, due to RB photosensitising properties, a case of severe systemic phototoxic reactions has been reported [46].

RBTF previously formulated were able to load RB increasing its *ex vivo* epidermis permeation and *in vitro* antiproliferative efficiency in melanoma cells (SK-MEL28), with a potential selectivity compared to normal cells (HFFF2) [39]. Furthermore, an optimal RBTF intradermal deposition was obtained after the inclusion in dissolving MNs [38]. Therefore, the current investigation aims to evaluate the RB pharmacokinetics and lymphatic uptake following intradermal deposition (i.d.) of RBTF. For the RB quantitative determination in biological fluids, the dissolving MNs were replaced with hollow MNs (HMNs) due to dissolving MNs poor drug loading capacity; compared to dissolving MNs that include all the therapeutic cargo in the microscopic polymer needle, HMNs deliver drugs through the drive of liquid pressure, similar to a conventional syringe. The main advantage of HMNs is the high drug delivery capacity, allowing continuous drug release with accurate dosing [13,32]. Herein, an *in vivo* study was performed on healthy rats, comparing RB's pharmacokinetics and lymph node accumulation following RBTF i.d.-HMNs to (i) RBTF dispersion administered *via* intravenous injection (i.v.), (ii) RB solution administered *via* i.d.-HMNs, and (iii) RB solution administered i.v.

2. Materials and methods

2.1. Materials

Rose Bengal disodium salt (RB), cholesterol, Span® 80, HPLC grade methanol, ammonium acetate, sodium hydroxide, phosphate-buffered saline (PBS) tablets (pH 7.3–7.5), dimethyl sulfoxide (DMSO) were purchased by Sigma-Aldrich (St. Louis, MO). Lipoid S100® was a kind gift from Lipoid GmbH (Ludwigshafen, Germany). Uranyl acetate (gadolinium acetate tetrahydrate) was purchased by Ted Pella Inc. (Redding, CA). Ethanol (industrial methylated spirit 99.5%) was obtained by Atomic Scientific (Manchester, UK). Ultrapure water was obtained from a water purification system (Elga PURELAB DV 25, Veolia Water Systems, Dublin, Ireland). Horse Serum was of UK origin and was obtained by Thermo Scientific (Hampshire, England). Nanosoft® HMNs were purchased from Fillmed (Paris, France).

2.2. Preparation and characterisation of RB-loaded transfersome (RBTF) dispersion

2.2.1. Preparation of RBTF dispersion

RBTF dispersion was prepared following the green protocol described in our previous works by modifying the quantitative composition [38,39]. First, the organic phase was constituted by dissolving Lipoid S100® (284 mg), cholesterol (52 mg) and Span® 80 (28 mg) in ethanol (5 mL) at 50 °C. The water phase was readily prepared by solubilising RB (40 mg) in ultrapure water (10 mL). Then, the organic phase was poured into the water phase, instantly forming a pink-milky dispersion. The resulting dispersion was homogenised by an ultrasonic probe (60 s, 50% ultrasound (US) amplitude) (Davidson & Hardy Ltd. cooperating with Fisher Scientific, Leicestershire, UK). Afterwards, ethanol was evaporated by rotary evaporation (50 °C) under vacuum (Rotavapor, Buchi Labortechnik, Switzerland). Finally, RBTF dispersion was further sonicated to achieve the desired RBTF dimensional profile. To do this, the ultrasonic device was set at 50% US amplitude for 3 min consisting of 10 s of US and 20 s of pause to avoid RBTF thermal

degradation. Unloaded TF (b-TF) were formulated likewise without adding RB to the water phase. RBTF and b-TF dispersions were stored in darkness at 4 °C.

2.2.2. RBTF and b-TF dimensional profile analysis

The dimensional profiles of RBTF and b-TF dispersions were evaluated regarding hydrodynamic diameter (nm) and polydispersity index (PDI). Based on the dynamic light scattering technique, a NanoBrook Omni particle sizer (Brookhaven, New York, USA) was used. Before each measurement, the dispersions were diluted with ultrapure water to guarantee that the concentration was in the required range of the instrument. The measurements were carried out in the following conditions: fluid refractive index 1.333; temperature 25 °C; viscosity 0.890 cP; scattering angle 90°; equilibration time 3 min; and sample run time 300 s. For RBTF dispersion, five batches were analysed in triplicate ($n = 15$); in the case of b-TF dispersion, three batches were analysed in triplicate ($n = 9$).

2.2.3. RBTF and b-TF morphology

At the end of the formulation processes, RBTF and b-TF dispersions were visualised by optical microscopy (Leica EZ4W stereomicroscope, Leica Microsystems, Milton Keynes, UK). Transmission electron microscopy (TEM) (Jeol JEM-1400 Transmission electron microscope, Welwyn Garden City, UK) was used to investigate the morphology of RBTF and b-TF vesicles. Before the analysis, one drop of RBTF and b-TF dispersions were separately pipetted on the top of a carbon copper grid and stained with uranyl acetate. Subsequently, the copper grids were gently washed with ultrapure water and dried at room temperature. Finally, the samples were analysed under TEM at the acceleration voltage of 120,000 V and magnification in the range of x1,000-x50,000. Images were visualised with a Jeol Ruby 8 MB bottom-mounted CCD camera.

2.2.4. Total drug in dispersion, drug loading and encapsulation efficiency

RBTF dispersion was evaluated for RB quantitative determination regarding the total drug in dispersion (RB% *w/v*), percentage drug loaded into the RBTF vesicle (DL%), and percentage encapsulation efficiency (EE%). RB quantitative analysis was carried out by High-Performance Liquid Chromatography (HPLC) coupled with a fluorescence detector (FLD) (Agilent Technologies 1220 Infinity UK Ltd., Stockport, UK). The chromatographic column employed was a C18 Phenomenex SphereClone™ column ODS (1) (150 × 4.6 mm i.d. with 5 µm particle size, pore size of 100 Å) (Phenomenex, Cheshire, UK). The method used is detailed in a previous article by the same authors [47]. To determine the total drug in dispersion, 50 µL of RBTF dispersion was added to 5 mL of methanol and kept under magnetic stirring for 20 min at 50 °C to ensure the RBTF dissolution. Then, 1 mL of the resulting mixture was taken and centrifuged for 15 min at 14,000 rpm (Sigma Laborzentrifugen GmbH, Osterode am Harz, Germany) before HPLC analysis. The total drug in dispersion (RB% *w/v*) was calculated as reported in eq. 1:

$$RB\left(\%\frac{w}{v}\right) = \frac{Total\ RB\ in\ dispersion(g)}{Volume\ of\ dispersion(mL)} \times 100 \qquad (1)$$

DL% and EE% were determined after removing free RB (non-encapsulated RB in RBTF vesicles) from the RBTF dispersion [48]. The free RB was removed by a dialysis method using a Float-A-Lyzer® G2 Dialysis Device (MWCO: 50 kDa, Spectra/Por®, Spectrum Laboratories, Inc. Rancho Dominguez, CA, USA). Briefly, 4 mL of RBTF dispersion were placed into the dialysis device and dialysed against PBS pH 7.4 (100 mL) under light magnetic stirring (48 h, 4 °C) [49]. Finally, the amount of RB dialysed, thus, free RB, was quantified and data used to calculate DL% and EE%, as indicated in eqs. 2 and 3, respectively:

$$DL\% = \frac{RB\ amount\ in\ dispersion(mg) - free\ RB(mg)}{Lipid\ phase(mg) + Total\ RB\ in\ dispersion(mg) + water(mg)} \qquad (2)$$

$$EE\% = \frac{Total\ RB\ in\ dispersion(mg) - free\ RB(mg)}{Total\ RB\ in\ dispersion(mg)} \times 100 \qquad (3)$$

For RB% *w/v*, DL%, and EE% determinations, three batches of RBTF dispersion were separately analysed in triplicate ($n = 9$). Moreover, two RB aqueous solutions (4 mg/mL) were dialysed following the same protocol described above as a control ($n = 6$).

2.2.5. In vitro release study

An *in vitro* release study was performed to evaluate the release profile of RB from RBTF dispersion using the dialysis method described in section 2.2.4 (50 kDa MWCO). RBTF dispersion (4 mL, RB ≈ 8 mg) was included in the dialysis device and placed in a cylindrical vessel containing PBS pH 7.4 as the acceptor medium (50 mL). The vessel was incubated at 37 °C and 50 rpm (SKI 4 Shaker Incubator, Argo Lab, Carpi, Italy). Samples of acceptor medium (1 mL) were collected throughout 24 h and analysed for RB amount using a UV–Vis spectrophotometer (Shimadzu UV-1800, Kyoto, Japan) referring to the calibration curve prepared in PBS pH 7.4 (RB excitation wavelength: 549 nm; standard solution range: 0.0015–0.017 mg/mL; y = 77.213×-0.067, R^2 = 0.9993). After each collection, the same volume of fresh medium was instantly replaced. Finally, the cumulative amount of RB released was plotted in the function of time. The experiment was performed by analysing three batches of RBTF dispersions ($n = 3$).

2.2.6. RBTF and b-TF physical stability

The physical stability of RBTF and b-TF dispersions was evaluated in terms of dimensional profile (size, PDI) (section 2.2.2) following 24 h of storage at 37 °C. Moreover, the dimensional profile of RBTF and b-TF was evaluated after 24 h of contact with 100% horse plasma (1:1) at 37 °C and 4 °C [50]. The experiment was performed by analysing three batches of b-TF and RB-TF dispersions ($n = 3$).

2.3. In vivo study

2.3.1. Design of the in vivo study

The *in vivo* pharmacokinetic study was approved by the Committee of the Biological Services Unit, Queen's University Belfast. The work was carried out under Project License PPL 2903 and Personal Licenses PIL 2127 and 2059. All experiments were conducted based on the policy of the Federation of European Laboratory Animal Science Associations and the European Convention for the protection of Vertebrate Animals used for experimental and other scientific purposes, implementing the principles of the 3Rs (replacement, reduction and refinement). The design of the *in vivo* study was schematised in Fig. 1.

Healthy female Sprague–Dawley rats (Charles River Laboratories, Harlow, UK) with an average weight of 280 g and aged between 10 and 12 weeks were acclimatised to the laboratory conditions for one week before starting the experiments. The rats ($n = 36$) were divided into six cohorts. Cohort n. 1 ($n = 6$) received a single intravenous (i.v.) injection of an RB aqueous solution (4 mg/mL) for an RB dosage of 4.0 mg/kg. Cohort n. 2 ($n = 6$) was administered with a single i.v. injection of an RBTF dispersion (RB = 4 mg/mL) for an RB dosage of 4.0 mg/kg. Cohorts n. 3 ($n = 6$) and 5 ($n = 6$) received a single administration of RB aqueous solution (RB = 4 mg/mL; 4.8 mg/kg) *via* intradermal (i.d.) injection; finally, cohorts n. 4 ($n = 6$) and 6 ($n = 6$) received a single administration of RBTF dispersion (RB = 4 mg/mL; RB = 4.8 mg/kg) *via* i.d. injection. In this investigation, i.d. injection was mediated by HMNs consisting of three needles with a length of 600 µm (Nanosoft® Microneedles, FillMed Laboratories, France) [51]. The 4.0 mg/kg dose was calculated based on the RB dosage used for treating metastatic melanoma in humans [52]. In the i.d. injection mediated by HMNs, a 4.8 mg/kg RB was administered as the device was estimated to retain about 20% of the formulation. The tested cohorts were first sedated through gaseous anaesthesia (2–4% isoflurane in oxygen). In the case of cohorts n. 3 to 6, the hairs from the rat backs were removed using electric hair
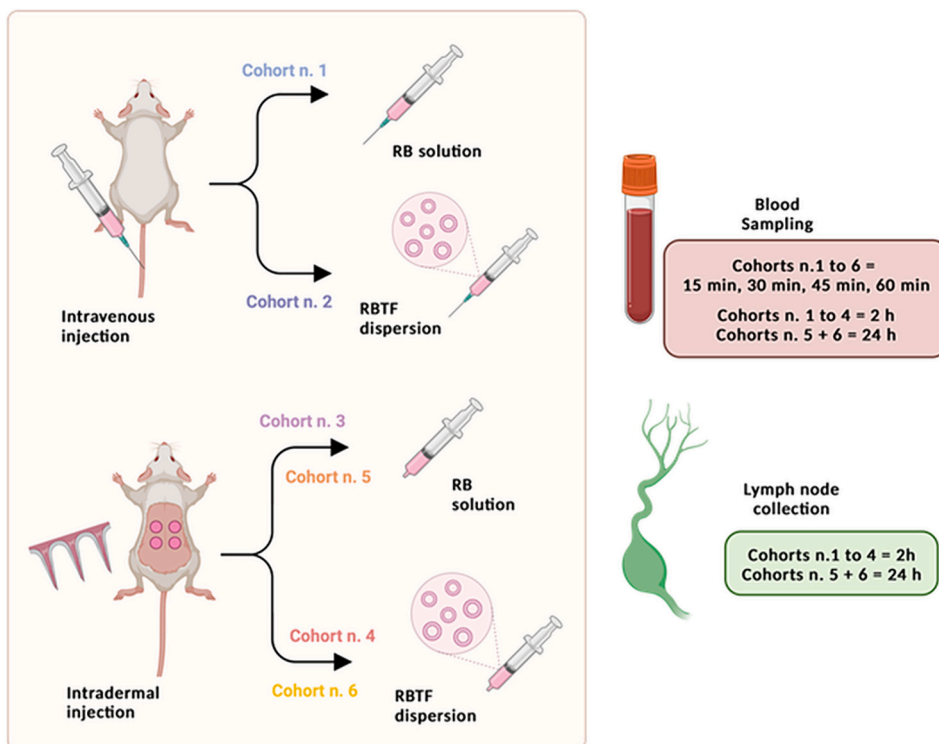
Fig. 1. The *in vivo* study design. The study was performed on female Sprague-Dawley rats ($n = 36$). Each cohort consisted of six rats ($n = 6$). Cohorts n. 1 and 2 received a single intravenous injection of RB solution and RBTF dispersion, respectively (4 mg/mL; 4 mg/kg). Cohorts n. 3 and 5 received a single intradermal injection of RB solution (4.0 mg/mL; 4.8 mg/kg) mediated by hollow microneedles (HMNs). Cohorts 4 and 6 received a single intradermal injection of RB solution (4.0 mg/mL; 4.8 mg/kg) mediated by HMNs. Blood samples were collected from all the cohorts after 15, 30, 45, and 60 min. Lymph nodes were collected following rat sacrifice: after 2 h (cohorts n. 1 to 4) or after 24 h (cohorts n. 5 and 6) of drug administration. Created with BioRender.com.

clippers (Remington Co., London, U.K.) and hair removal cream (Sodalis Srl, Milano, Italy). Then, the animals were left to rest for 24 h before administering the formulations to ensure the skin barrier recovery that could have been altered by the epilation process [53]. Afterwards, rats were sedated again (2–4% isoflurane in oxygen), HMNs were applied to their backs, and the formulations were injected with a syringe directly connected to the HMN device (Fig. 2).

Blood samples were taken *via* tail vein bleeds at predetermined time points (15, 30, 45, and 60 min) with a maximum of 200 μL collected at each sampling point and stored in pre-heparinised microtubes. Subsequently, all the rats in cohorts n. 1 to 4 were sacrificed after 2 h of drug administration by cardiac puncture, the blood was sampled, and lymph nodes (axillary and popliteal) were harvested. Similarly, all the rats belonging to cohorts n. 5 and 6 were sacrificed after 24 h of the drug administration by cardiac puncture, the blood was sampled, and lymph

nodes (axillary and popliteal) were harvested. Finally, blood samples and lymph nodes were processed for RB quantitative studies. Blood samples were subjected to an RB extraction process to quantify the analyte in the systemic circulation and evaluate the pharmacokinetic profile. The harvested lymph nodes were processed to extract the analyte and quantify the RB amount accumulated. The protocols for extracting and quantitatively determining RB from plasma and lymph nodes are described in sections 2.3.2 and 2.3.3, respectively.

2.3.2. RB extraction from plasma

The blood samples from rats were centrifuged at 3000 rpm at 4 °C for 15 min using a Sigma 2-16 K centrifuge (Osterode am Harz, Germany). A 100 μL aliquot of the plasma supernatant was collected and transferred to an Eppendorf tube containing 800 μL of methanol. The tubes were vortexed at 1500 rpm for 30 min and then centrifuged at 14,800 rpm at 4 °C for 10 min. Next, 800 μL of the supernatant was transferred to a glass tube and placed in a nitrogen evaporator (Zymark Corporation, Hopkinton, Massachusetts, USA) at 40 °C until all the solvent was evaporated entirely. Subsequently, 300 μL of methanol was added to the glass tube to reconstitute RB. The solution was transferred to HPLC vials for further quantification using the method previously described and suitability modified [47].

2.3.3. RB extraction from lymph nodes

RB in the lymph node samples was quantified using the same technique previously reported for RB extraction from the skin, with a slight modification [47]. The lymph nodes were cut into small pieces and transferred to an Eppendorf tube containing 0.5 mL of deionised water and two stainless steel beads (diameter = 0.5 cm) (Qiagen, Hilden, Germany). The samples were lysed using a Qiagen TissueLyser® LT (UK Qiagen Ltd., Manchester, UK) at 50 Hz for 15 min. After that, 1 mL of DMSO was added to the samples, followed by another lysis cycle. The
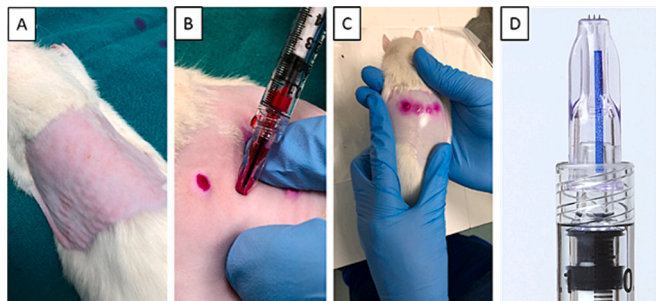
Fig. 2. Intradermal (i.d.) administration of RBTF dispersion assisted by HMNs. A. Rat's back after hair removal. B. i.d. administration of RBTF dispersion. C. Rat's back after RBTF i.d. administration. D. Zoom of the HMN device used for i. d. administration (600 μm Nanosoft® Microneedles, FillMed Laboratories, France).

samples were centrifuged at 14,800 rpm for 10 min, and the supernatant was collected. If necessary, the samples were diluted with DMSO before injection into the HPLC system using the method previously described and suitability modified [47].

2.3.4. Pharmacokinetic data analysis

Pharmacokinetic (PK) evaluation was done using PKSolver, an add-in program for PK data analysis in Microsoft Excel® 2013 [54]. Non-compartmental model analysis was applied. PK parameters analysed were: RB maximum plasma concentration (C_{max}); time of the maximum concentration (T_{max}); the AUC from time zero ($t = 0$) to the last experimental point, which was 2 h regarding cohorts n. 1 to 4 (AUC_{0-2}) and 24 h for cohorts n. 5 and 6 (AUC_{0-24}); the AUC from time zero ($t = 0$) until infinity (AUC_{0-inf}); the mean half-life ($t_{1/2}$); the mean residence time (MRT). The AUC_{0-2} and AUC_{0-24} were calculated by the linear trapezoidal method [53,55].

2.4. Statistical analyses

All the numerical data herein reported are expressed as mean value ± standard deviation of at least $n \geq 3$ experimental measures, calculated using GraphPad Prism® 10.0.0 (153) (GraphPad® Software, San Diego, USA). The same software was used to analyse the data set regarding statistical significance. The statistical method employed for the singular data sets was indicated in section 3. Results and Discussion; it was chosen based on the GraphPad Prism® user guide [56]. A *p*-value≤0.05 was considered for statistical significance in all cases.

3. Results and discussion

3.1. Preparation and characterisation of RBTF dispersion

RBTF dispersion was first developed using a green reverse-phase evaporation method [39] and then optimised for inclusion in MN systems [38]. The RBTF dispersion prepared herein does not differ for process parameters and excipients-drug ratio concerning the previous investigation [38]. At the end of the formulation process, no phase separation or naked-eye visible aggregates were observed. A turbid white dispersion was obtained in the case of b-TF dispersion (Fig. 3A); the RBTF one appeared pink-coloured due to RB addition and was more transparent (Fig. 3B). The dimensional profile analysis (Table 1) pointed out that both formulations were nanosized and vesicles uniformly distributed (PDI < 0.4). However, a significant difference in terms of size was detected when comparing the two dispersions. RBTF vesicles were significantly smaller than b-TF ones (*p*-value<0.0001): RBTF ranged from 82.31 to 110.23 nm, whereas b-TF ranged from 170.93 to 204.59 nm. The turbidity of the dispersions predicted these observations per the Tyndall effect [57,58]. A further dissimilarity was noticed in the

Table 1

Dimensional profile of RBTF and b-TF dispersions (RBTF dispersion: $n = 15$, five batches analysed in triplicate; b-TF dispersion: $n = 9$, three batches analysed in triplicate).

	Size (nm)	PDI
RBTF dispersion	96.27 ± 13.96[†]	0.29 ± 0.02
b-TF dispersion	187.76 ± 16.83[†]	0.19 ± 0.01

[†] RBTF dispersion vs b-TF dispersion: p-value < 0.0001 (unpaired t-test, two-tailed).
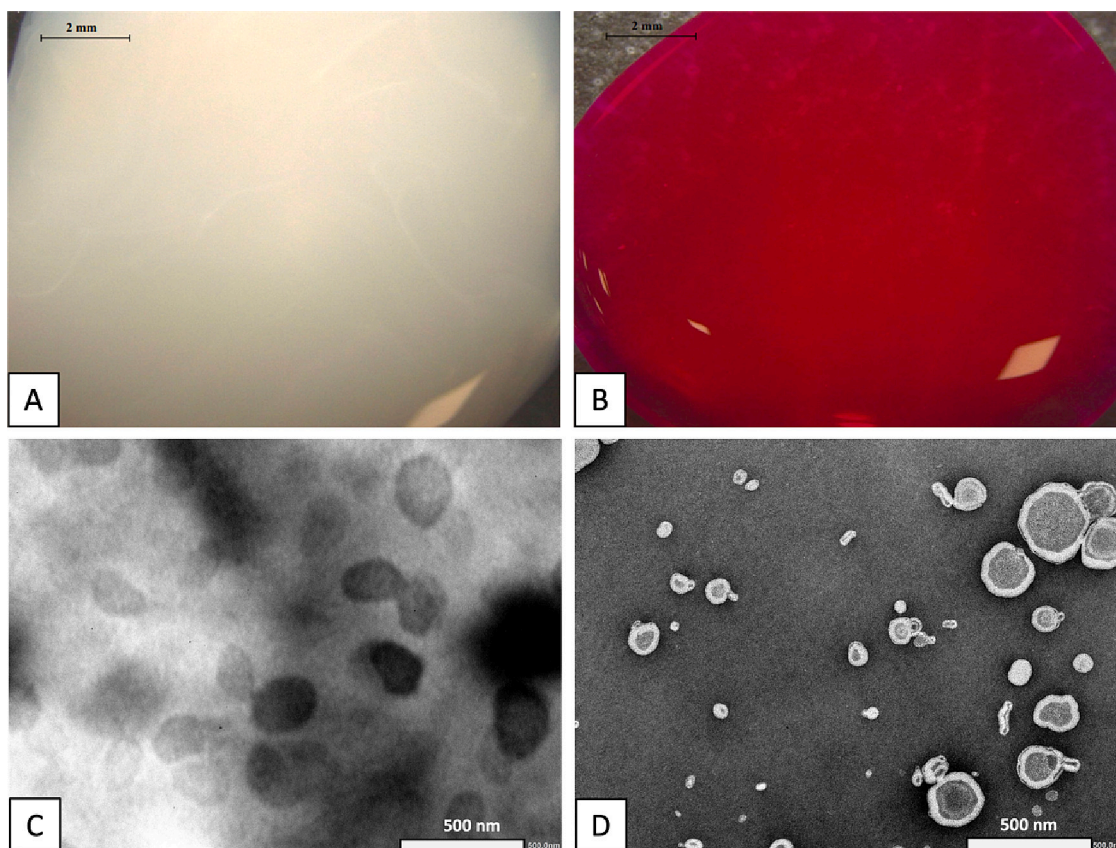
Fig. 3. Appearance and morphology of b-TF and RBTF dispersions. **A-B**: Images acquired by optical microscopy (2 mm bar; magnification 8×); A. b-TF dispersion; B. RBTF dispersion. **C-D**: Images acquired by TEM (500 nm bar); C. b-TF dispersion (magnification x25k); D. RBTF dispersion (magnification x25k).

morphology of RBTF and b-TF vesicles. As shown in Fig. 3C, b-TF vesicles seem to have an oval shape, elongated; also, the double layer, characteristic of liposome-like vesicles, is slightly visible and hard to appreciate. On the contrary, RBTF vesicles (Fig. 3D) are round-shaped, and the double layer is evident, easily distinguishable, and thick. Moreover, some vesicles appear multilamellar.

The outcomes reported above indicate RB's pivotal role in the dimensional and structural features of RBTF. RB is a water-soluble molecule and displays moderate hydrophobicity (logP = 0.59). As a result, its affinity for lipids is expected and documented in the literature [59–61]. Further, RB carries two ionisable groups that are predominantly found in the deprotonated form starting from a pH value of ≈6.3 [62] (Fig. 4A). RB is an emerging drug, and little is known about its behaviour with biological membranes, which is comparable, in terms of structure, to the bilayer of liposomal vesicles. We previously reported that in the case of RBTF vesicles, which are prepared at basic pH values, RB intercalates beneath the phospholipid palisade, modifying the lipid packing parameter and, consequently, the characteristics it regulates, such as lamellarity, vesicle's hydrodynamic diameter and size distribution [39,63]. More recently, the RB's interaction with biological membranes has been evaluated on mammalian phospholipid bilayer models by Sztandera et al. [62]. The investigation clarified that the deprotonated groups of RB strongly interact with the positively charged amine groups of hydrophilic lipid heads localised in the membrane's outer surface; on the contrary, moderate-to-no interactions with hydrophobic chains and alterations in lipid order parameter were noticed (Fig. 4B) [62]. The latter point apparently disagrees with our findings; however, it is of considerable importance that Sztandera et al. investigated RB interaction with a preformed lipid bilayer, whereas, in the current investigation, RB was forced to interact with single lipid molecules during the formulation process, to finally form a lipid bilayer that it is likely to include RB (Fig. 4C). The nature of this inclusion still needs to be elucidated. However, it is hypothesised to be correlated to the temperature at which RBTF are prepared (50 °C) compared to the lower temperature of Sztandera et al. contribution [64].

Sztandera et al. observed that the interactions between RB and hydrophilic moieties were sufficiently strong to maintain RB anchored to the lipid bilayer [62]. This agrees with the data presented herein regarding DL%, EE%, and *in vitro* release profiles (Fig. 4D, Table 2). The

Table 2
Quantitative determination of RB in RBTF dispersion ($n = 9$, three batches analysed in triplicate).

Total drug in dispersion (% w/v)	0.35 ± 0.02[†]
Drug Loading (%)	0.33 ± 0.02[†]
Encapsulation Efficiency (%)	98.54 ± 0.09

[†] Total drug in dispersion vs Drug Loading: p-value < 0.05 (unpaired t-test, two-tailed).

DL% (RB encapsulated into RBTF vesicles) was close to the value of the total drug in dispersion (free RB + encapsulated RB) (p-value = 0.024) (Table 2). Remarkably, the dialysis test performed on RBTF dispersion revealed that an RB percentage of 1.46 ± 0.09 was quantified in the acceptor medium and related to non-encapsulated RB. The data is unaffected by RB's inability to pass through the dialysis membrane, as 100% of the drug was quantified in the acceptor medium over the same time during the control test (Fig. 4, D1). This means that most RB added to prepare RBTF dispersion is somehow associated with RBTF vesicles, resulting in an EE% higher than 98% (Table 2). Similar results were acquired when evaluating RBTF dispersion for *in vitro* RB release (Fig. 4, D2); in this case, 1.43 ± 0.11 % RB was released over 48 h of incubation at 37 °C, suggesting RB remains anchored to the RBTF vesicle even at physiological conditions.

Lastly, the physical stability of RBTF and b-TF dispersions was evaluated regarding the dimensional profile when incubated for 24 h at 37 °C; the testing time was selected based on the duration of the *in vivo* study (24 h) (section 2.8.1). Furthermore, although RBTF vesicles were designed to favour lymphatic accumulation, the stability in plasma was investigated since it may provide unique preliminary information about RBTF behaviour *in vivo*. The results of physical stability are summarised in Fig. 5. Notably, the size of RBTF and b-TF vesicles did not vary when exposed to 37 °C, suggesting that they could maintain their size and structure *in vivo*. Nevertheless, the size of RBTF decreased after incubation with plasma at 37 °C and 4 °C; another case of the reduced size of liposome-like vesicles after plasma contact was reported by Ding and collaborators [50]. The original RBTF size was 96.27 ± 13.96 nm. After 24 h of contact with plasma at 37 °C, the size decreased to 74.4–89.45 nm range (p-value = 0.018). At 4 °C the size reduction was more pronounced (69.8–89.54 nm; p-value = 0.004) (Fig. 5B). As the literature
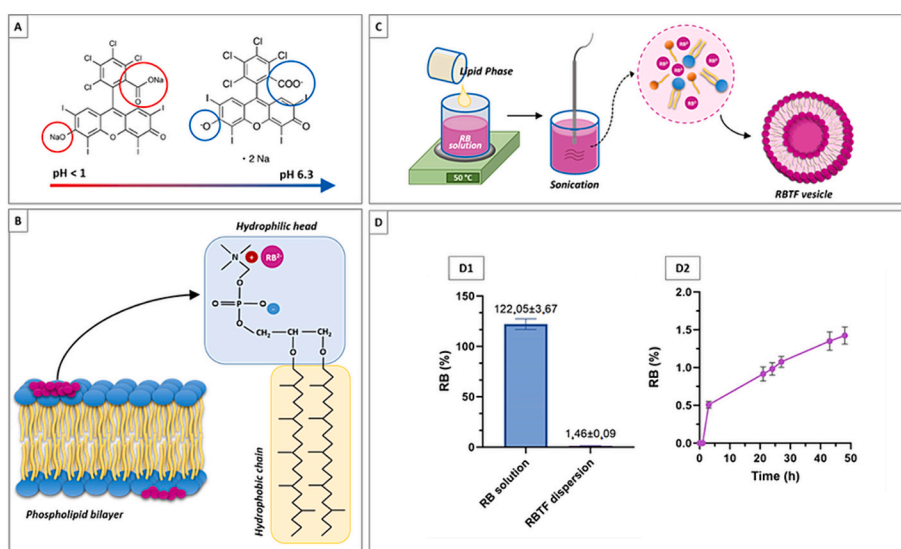
Fig. 4. Interaction mechanism of RB with lipid phase. **A.** RB ionisation states at acidic and basic pH. **B.** Negative RB interacts with positive amine groups of phospholipid's hydrophilic heads localised on the outer surface of mammalian membranes. **C.** Interaction of RB and phospholipids molecules during RBTF preparation process: a scheme in brief. **D1.** Percentage of RB dialysed from RB solution and RBTF dispersion over 48 h against PBS pH 7.4 (4 °C) (RBTF dispersion: $n = 9$, three batches analysed in triplicate; RB solution: $n = 6$, two batches analysed in triplicate). **D2.** Percentage of RB released (dialysed) from RBTF dispersion over 48 h against PBS pH 7.4 (37 °C) ($n = 3$, three batches analysed once).
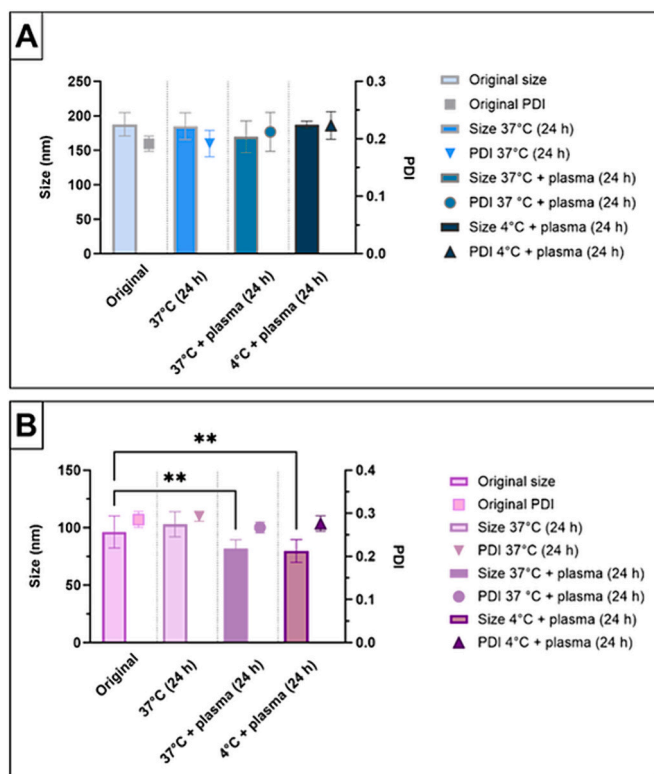
Fig. 5. Physical (dimensional) stability of b-TF and RBTF dispersions at different storage conditions. **A.** b-TF stability; **B.** RBTF stability. Format data table: columns. RBTF original size and PDI: $n = 15$, five batches analysed in triplicate; other samples: $n = 9$, three batched analysed in triplicate—Statistical analysis by Prism® multiple comparisons, Kruskal-Wallis uncorrected Dunn's test (each comparison stands alone): the mean rank of size 37 °C, size 37 °C + plasma and size 4 °C + plasma was compared with the mean rank of the original size.

suggests, this result could be related to the interaction of plasma proteins with the outer surface of the RBTF, the so-called "protein corona" phenomenon [65]. The experimental method herein applied did not intend to predict the *in vivo* formation of the protein corona; indeed, the *in vitro* surrogate is insufficient for that scope. Still, this hypothesis may explain the different behaviour of RBTF compared to b-TF vesicles. In fact, in the latter case, no difference was noted after the incubation with plasma, regardless of the temperature (Fig. 5A). The apparent dimensional stability of b-TF in plasma may be attributed to their neutral surface charge (-4.9 ± 0.9 mV), documented in the previous investigations, in contrast to the negative surface of RBTF vesicles (-45.90 ± 0.85 mV) [38,39]. It was seen that plasma proteins display a higher affinity to charged liposomes compared to neutral ones. Mainly, negatively charged liposomes prefer interacting with basic plasma proteins, while positively charged ones tend to interact with acidic proteins [50,65].

In summary, the prepared RBTF vesicles showed a size around 100 nm, suitable for lymphatic targeting, with a uniform distribution profile. RBTF encapsulated most of the RB added during the preparation and did not release RB at simulated physiological conditions. The no-release properties may allow RBTF to efficiently interact with circulating cancer cells based on a selectivity conferred by the drug [42,66]; also, considering RB fluorescence properties, this would enable the tracking of RBTF for biodistribution purposes [47]. Furthermore, RBTF vesicles maintained their dimensional profile unchanged, even if the size (nm) slightly decreased when in contact with the plasma. Based on these outcomes, RBTF dispersion was considered a promising candidate to favour a lymphotropic delivery of RB and was evaluated for pharmacokinetic and lymph node accumulation *in vivo*.

3.2. In vivo study

The *in vivo* study was performed on healthy Sprague Dawley rats as an animal model. RB solution and RBTF dispersion were administered separately through intravenous (i.v) and intradermal (i.d) routes. The rats showed no signs of pain, swelling, or irritation during the experiment. Results will be presented in terms of pharmacokinetic analysis of RB, comparing its profile across different administration routes and formulations, with a statistical robustness ensured by the applied statistical methodologies suitable for the data set. Finally, a discussion section will comment on the pharmacokinetic findings highlighting the potential implications and innovative aspects of the study.

3.2.1. Pharmacokinetics, lymph-node accumulation, and statistical analysis

Results of the *in vivo* study have been graphically resumed as follows: Fig. 6 displays the plasma concentration profiles of RB following i.v. and HMNs-assisted i.d. administrations of both RB solution and RBTF dispersion. Table 3 and Fig. 7 summarise the pharmacokinetic parameters. Fig. 8 illustrates the amount of RB accumulated in the lymph nodes at the end of the *in vivo* study.

The observed pharmacokinetic parameters indicate a potential improvement in the systemic circulation of RB when encapsulated in RBTF, suggesting that this strategy may enhance RB's pharmacokinetic profile, especially evident when comparing these findings to data reported in the literature [45]. Upon i.v. administration, not only RBTF did exhibit a marked prolongation of RB $t_{1/2}$ to 1.35 ± 0.34 h compared to 0.52 ± 0.08 h for the RB solution (p-value = 0.0156), but also significantly increased the MRT$_{0\text{-inf}}$ to 1.67 ± 0.02 h, nearly three times the duration observed with the RB solution. Klaassen et al., reported an initial biological half-life of 2 min and a terminal half-life of 100 min for RB doses ranging between 0.01 and 10 mg/kg in rats, with a biological half-life for excretion around 30 min [45]. These observations suggest that TF may have the capability to enhance RB's retention in the systemic circulation, potentially facilitating a more prolonged therapeutic action.

The AUC and half-life for both RB formulations administered i.d. notably exceeded those observed for i.v. routes, underscoring the effectiveness of i.d. delivery in sustaining drug levels over time. Particularly, RBTF i.d. administration achieved an AUC$_{0\text{-inf}}$ of 2158.62 ± 292.01 ng/mL*h, significantly higher than that observed for RB solution i.d. 1037.57 ± 138.17 ng/mL*h, and nearly twofold the AUC reported by Klaassen. The data suggest that RBTF, when i.d. administered, tends to achieve plasma concentrations that are notably superior to those observed with i.v. RB solutions, indicating a possible advantage of i.d. administration, with a 50-fold increase after 24 h of treatment (p-value = 0.0340) and an 18-fold rise over i.v. RBTF dispersions (p-value = 0.0440). This result demonstrates the TF's effectiveness in permeating biological barriers to deliver RB efficiently into the systemic circulation.

The observed T$_{max}$ for RB solution i.d. (0.56 ± 0.31 h) is superior to that for RBTF i.d. (0.31 ± 0.13 h), which may be attributed to the differential absorption dynamics governed by TF. The TF's design facilitates a quicker entry into the systemic circulation, whereas the RB solution may take longer to peak concentration. This difference in T$_{max}$ between the formulations highlights the importance of the delivery system in dictating the absorption rate and bioavailability of administered drugs.

The present results suggest that the use of RBTF for RB delivery markedly improved the drug's pharmacokinetic profile, offering a significant advancement over traditional delivery methods. The observed prolonged half-life, increased AUC, and C$_{max}$ with TF utilisation underscore the promising potential of NCs systems in advancing drug delivery and efficacy, warranting further investigation, particularly for chemotherapeutic agents where controlled release is critical to maximising therapeutic outcomes using low doses to reduce the collateral effects. In this case, the i.d. application using HMNs with RBTF reduced
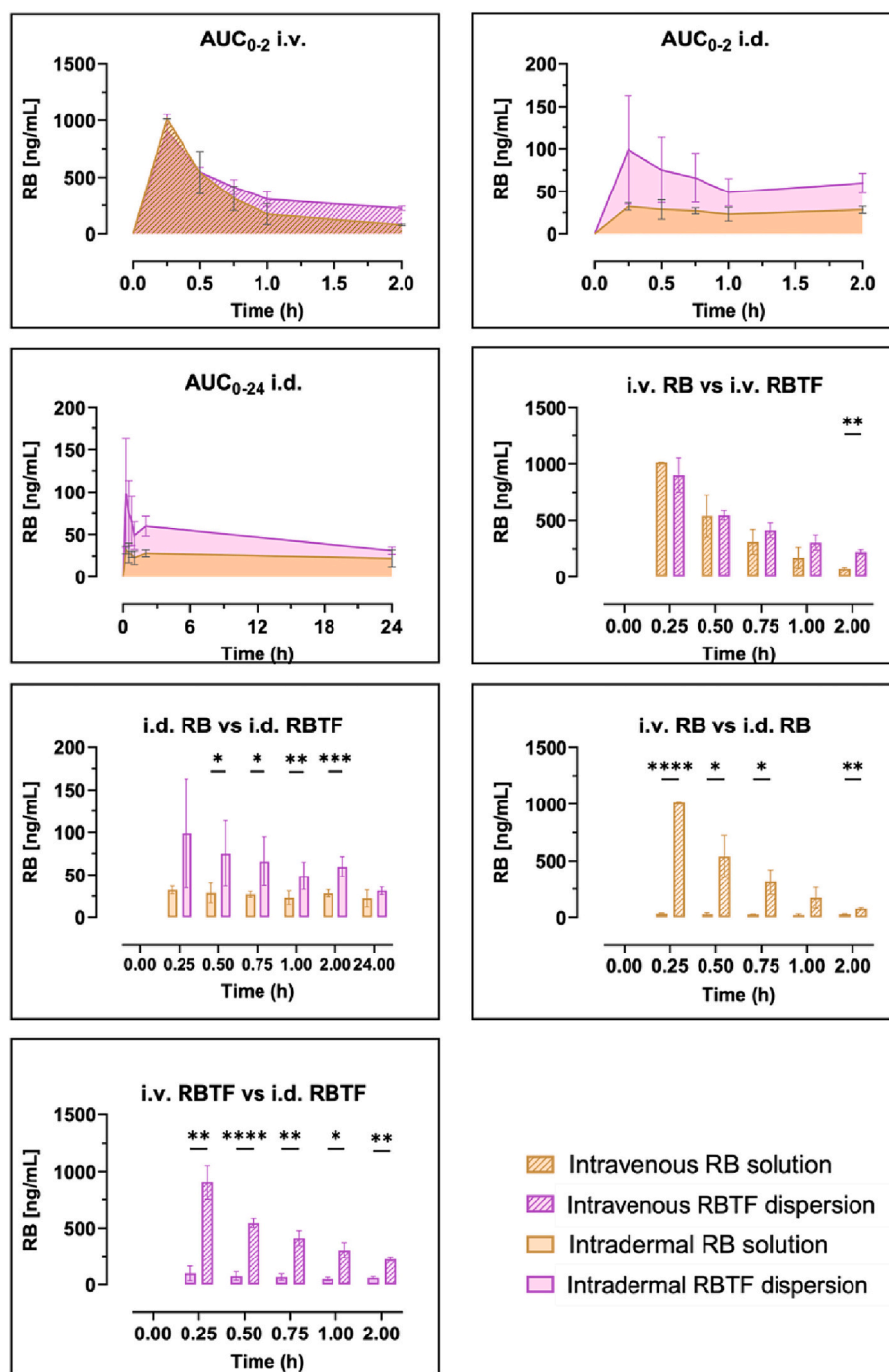
Fig. 6. RB plasma concentration and relative statistical comparisons after intravenous (i.v.) (RB = 4.0 mg/kg) or intradermal (i.d.) (RB = 4.8 mg/kg) injection of RB solution and RBTF dispersion. Format data table: XY, two groups, time points separated per row. Intravenous RB and RBTF: $n = 3$, three rats were analysed per blood sampling point; Intradermal RB and RBTF: $n = 6$, six rats were analysed per blood sampling point—Statistical analysis by Prism® Two-Way ANOVA, mixed-effects model, Geisser-Greenhouse correction, matched values stacked into sub-columns, individual variance computed for each comparison.

the dose, improved the lymphatic uptake, prolonged the main residence time, obtaining higher AUC when compared to the other groups.

Finally, RB accumulation in lymph nodes was quantified at the end of the animal study. RB was not detected in popliteal lymph nodes. Fig. 8B reports the RB amount found in axillary lymph nodes. As shown, in the case of i.v. RB solution, no RB was detected in the lymph node; still, RBTF dispersion resulted in an accumulation of 12.3 ± 0.14 ng/mL RB after 2 h. On the contrary, HMNs-assisted i.d. administration promoted RB accumulation in lymph nodes. Regarding i.d. RB solution, no RB was detected after 2 h, but only after 24 h (13.3 ± 1.41 ng/mL). The

administration of RBTF resulted in the most significant RB accumulation after 2 h of injection, visible to the naked eye (Fig. 8A), reaching the value of 84.2 ± 25.10 ng/mL, which decreased to 22.9 ± 8.49 ng/mL at 24 h.

3.2.2. Discussions of findings

The results presented suggest several assumptions: (i) free RB has limited capacity in permeating biological tissues, (ii) RBTF may enhance RB's *in vivo* biopharmaceutical profile, and (iii) RBTF could represent an efficient lymphotropic delivery system for RB, though further studies are

Table 3
Calculated pharmacokinetic parameters for RB after intravenous (i.v.) and intradermal (i.d.) administration of RBTF dispersion or RB solution (for i.v. administration $n = 3$, three rats analysed per each blood sampling point; for i.d. administration $n = 6$, six rats analysed per each blood sampling point).

Parameter	Unit	RB solution i.v.	RBTF dispersion i.v	RB solution i.d.	RBTF dispersion i.d
$t_{1/2}$	h	0.52 ± 0.08	1.35 ± 0.34	26.92 ± 8.66	24.08 ± 4.74
t max	h	0.25 ± 0.00	0.25 ± 0.00	0.56 ± 0.31	0.31 ± 0.13
C max	ng/mL	1012.03 ± 3.3	902.45 ± 150.67	35.51 ± 8.53	100.24 ± 28.73
AUC 0-t	ng/mL*h	876.16 ± 128.70	959.78 ± 94.26	529.65 ± 87.80	1121.00 ± 123.56
AUC 0-inf	ng/mL*h	934.70 ± 140.70	1392.13 ± 180.95	1037.57 ± 138.17	2158.62 ± 292.01
MRT 0-inf	h	0.573 ± 0.03	1.67 ± 0.02	37.73 ± 12.43	32.63 ± 5.96

needed to confirm these findings.

(i) Free RB has limited capacity in permeating biological tissues.

The lowest RB peak plasma concentration was observed for RB solution after i.d. administration: ≈ 35 ng/mL i.d. *vs* ≈ 1010 ng/mL i.v. after 15 min. The considerable difference between the two routes is relatable to the poor ability of RB to permeate across biological membranes if not formulated in a suitable delivery system [40,47,62]. Indeed, the high molecular weight and the amphiphilic nature of the drug represent an issue for a consistent permeability. Some RB systemic absorption was noticed after i.d. injection, which is reasonable considering RB's physical-chemical profile and skin characteristics [67]. Indeed, skin comprises an outmost hydrophobic barrier (*stratum corneum*, SC) which protects the underneath tissues (viable epidermis and dermis). Based on the transdermal hydration gradient, while going more profound in the viable epidermis and dermis, the skin gradually becomes water-rich and hydrophilic, reaching a water percentage of $\approx 70\%$ in the dermis of healthy young subjects 68. In this investigation, the highly water-soluble RB was deposited by HMNs directly into the dermis, bypassing the SC barrier, the main obstacle for RB skin permeation. In this way, RB may easily permeate through the dermis, finally reaching blood capillaries for uptake. This last step likely represented the main limitation for RB systemic absorption after i.d. administration. In truth, free RB interacted with mammalian cells' outer surface, but it cannot permeate it and reach the inner side [62], supporting the hypothesis herein designed. However, even if the i.d. delivery efficiency of free RB was poor, two advantages over the i.v. route were observed, that were the longest RB $t_{1/2}$ and MRT, suggesting that i.d. administration assisted by HMNs may control RB absorption rate.

(ii) i.d. RBTF enhance RB's *in vivo* biopharmaceutical profile.

After the administration of RBTF, several RB improvements were noticed, starting from the i.v. route. The RB i.v. $t_{1/2}$ resulted in ≈ 30 min. After RBTF i.v. injection, $t_{1/2}$ increased to ≈ 80 min; similarly, MRT_{0-inf} was much more significant for RBTF i.v. than RB i.v. The short circulatory half-life of RB was expected based on the drug's high water solubility and agrees with previous observations [45,69]. However, this main drawback was solved by loading RB in the lipid RBTF vesicle, which were previously proved to control RB release firmly (section 3.1). Furthermore, the literature reports that NPs smaller than 260 nm can escape macrophages' clearance, prolonging the blood circulation time [70]. Regarding RB delivery by HMNs assisted i.d. injection, RBTF could ensure a higher RB plasma concentration over RB

solution at each sampling point, confirming the high efficiency of TF as delivery system conventionally ascribed to their deformability properties. TF are flexible liposomal vesicles that pass through the tiny skin pores keeping their original structure and minimising drug loss. Due to the presence of a water core, TF naturally tend to avoid dry surroundings. Thus, the driving force for the migration through the skin is produced by transdermal hydration gradient. As a result, they can reach dermis capillaries and finally enter the blood [23,24,71].

(iii) RBTF are an efficient RB lymphotropic delivery system.

In agreement with points (i) and (ii), i.v. RB solution did not provide any RB accumulation in lymph nodes. Conversely, RBTF demonstrated a potential tool to reach that goal, particularly following i.d. route. The more significant and faster accumulation for i.d. RBTF compared to i.v. RBTF is highly probable to result from the different administration routes combined to RBTF size. Indeed, administering the formulation directly in the systemic circulation is naturally advantageous for 100% bioavailability, but limits, to some extent, the lymphatic targeting consequent to a generic biodistribution. In contrast, the skin represents a suitable administration site for lymphotropic delivery due to the high density of lymph capillaries, enabling lymphotropic delivery even in the case of i.d. RB solution [20,72,73]. Furthermore, based on the literature, the size of RBTF (≈ 100 nm) played a key role. As stated in the introduction, NPs in the 10–150 nm range preferentially enter lymph than blood capillaries [22,74]. This phenomenon is related to the different blood and lymph capillary wall gap sizes. Indeed, blood vessels are composed of endothelial cells attached by gap junctions, whereas weaker junctions connect lymphatic endothelial cells. Also, the basal membrane of blood capillaries comprises lining cells, not present in the case of lymphatic capillaries, which prevent the uptake of particles larger than 10 nm [22].

4. Conclusion

Herein, we are reporting for the first time, the improved pharmacokinetic and lymphatic delivery of Rose Bengal (RB) using transferosomes administered intradermally by hollow microneedles. The current study aimed to develop a strategy to boost the lymphotropic delivery and pharmacokinetics of the hydrosoluble chemotherapeutic RB based on the pivotal role played by the lymphatic system in the progression of cancer metastases. To do this, deformable liposome-like vesicles were prepared and loaded with RB, an emerging but efficient anticancer molecule. RBTF improved the pharmacokinetic profile of RB by prolonging the blood circulation time. More importantly, RBTF (100 nm size) accumulated in healthy rats' lymph nodes when delivered intradermally using hollow microneedles (HMNs). Lastly, HMNs were herein used to prove this theory, considering the drug loading challenge previously faced with dissolving MN patches; however, developing a polymeric MN array with more needles and a larger surface area would potentially improve patient treatment. In this point of view, we intend to focus the following studies on the optimisation of dissolving microneedle design loading nanoparticles. The outcomes reported suggest that RBTF may become a valid tool for metastatic cancer therapy. To evaluate the pharmacological potential, a pharmacodynamic study on tumorigenic animal models will be conducted in a future investigation.

CRediT authorship contribution statement

Sara Demartis: Writing – review & editing, Writing – original draft, Visualization, Validation, Methodology, Investigation, Formal analysis, Conceptualization. **Giovanna Rassu:** Writing – review & editing, Validation, Supervision, Methodology. **Qonita Kurnia Anjani:** Writing – review & editing, Validation, Methodology, Investigation. **Fabiana Volpe-Zanutto:** Writing – review & editing, Validation, Methodology,
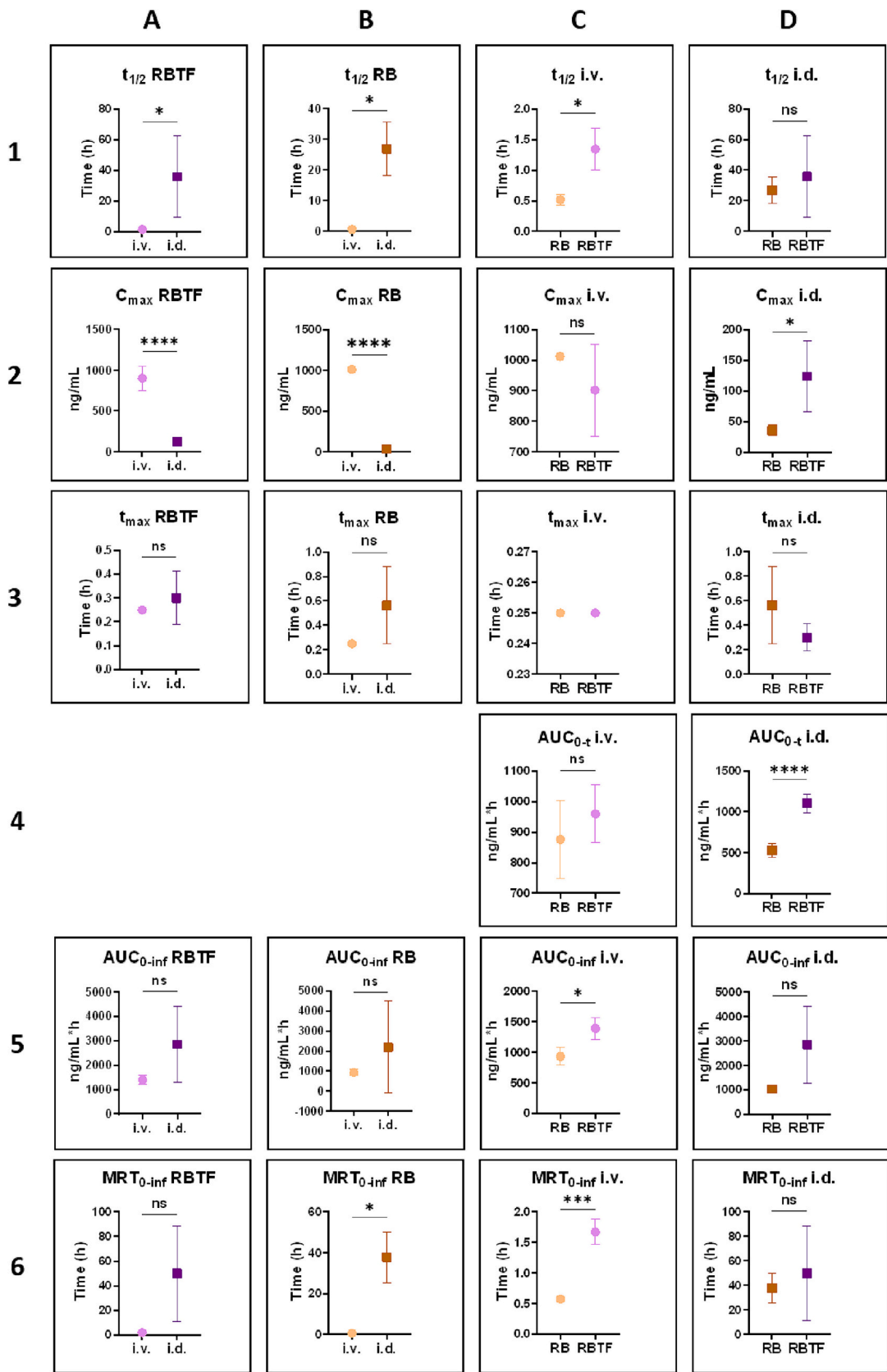
Fig. 7. Statistical analysis of the calculated pharmacokinetic parameters obtained from the *in vivo* study. **Columns: A:** intravenous (i.v.) *vs* intradermal (i.d) injection of RBTF dispersion. **B:** i.v. *vs* i.d injection of RB solution. **C:** i.v. RB solution *vs* i.v. RBTF dispersion. **Column D:** i.d. RB solution *vs* i.d. RBTF dispersion. Format data table: column. Intravenous RB and RBTF: n = 3, three rats were analysed per sampling point; Intradermal RB and RBTF: n = 6, six rats were analysed per sampling point—statistical analysis by Prism® parametric unpaired t-test with Welch's correction (do not assume equal SDs).

Formulation	2 h	24 h
RB i.v.	not detected	Not detected
RBTF i.v.	12.80±0.14	Not detected
RB i.d.	not detected	13.30±1.41
RBTF i.d.	84.20±25.10	22.90±8.49
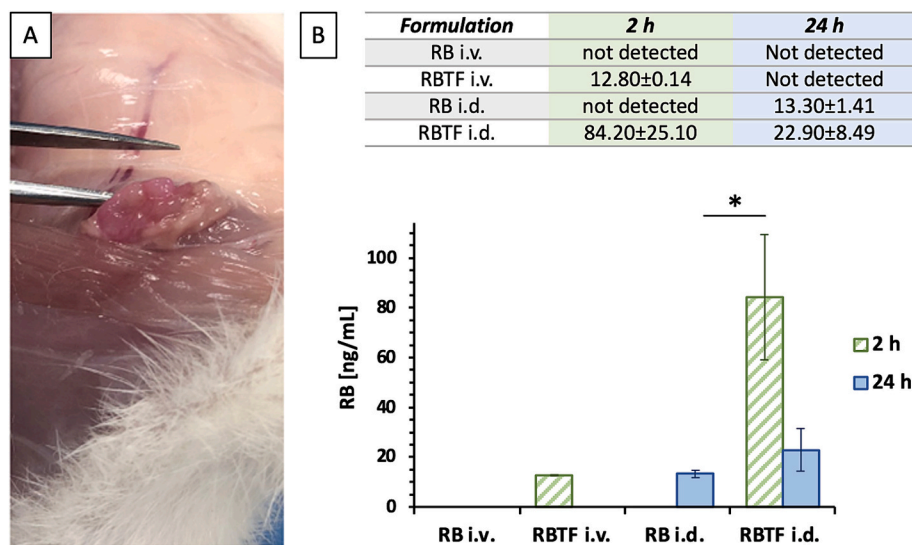
Fig. 8. RB accumulation in axillar lymph nodes following intravenous (i.v.) and intradermal (i.d.) injection of RB aqueous solution and RBTF dispersion. **A.** pink-coloured lymph node harvested after 2 h of RBTF administration *via* i.d. route. **B.** RB concentration in lymph nodes when harvested after 2 h and 24 h of drug administration. Format data table: column; $n = 3$, three rats were analysed per sampling point;—statistical analysis by Prism® parametric unpaired *t*-test with Welch's correction (do not assume equal SDs). (For interpretation of the references to colour in this figure legend, the reader is referred to the web version of this article.)

Declaration of competing interest

The authors declare no competitive interest.

Data availability

Data will be made available on request.

Acknowledgements

References

[1] G. Oliver, J. Kipnis, G.J. Randolph, N.L. Harvey, The lymphatic vasculature in the 21st century: novel functional roles in homeostasis and disease, Cell 182 (2020) 270–296, https://doi.org/10.1016/j.cell.2020.06.039.

[2] H. Ji, C. Hu, X. Yang, Y. Liu, G. Ji, S. Ge, X. Wang, M. Wang, Lymph node metastasis in cancer progression: molecular mechanisms, clinical significance and therapeutic interventions, Sig Transduct Target Ther 8 (2023) 367, https://doi.org/10.1038/s41392-023-01576-4.

[3] R. Shayan, M.G. Achen, S.A. Stacker, Lymphatic vessels in cancer metastasis: bridging the gaps, Carcinogenesis 27 (2006) 1729–1738, https://doi.org/10.1093/carcin/bgl031.

[4] A. Taheri, K.E. Bremmell, P. Joyce, C.A. Prestidge, Battle of the milky way: lymphatic targeted drug delivery for pathogen eradication, J. Control. Release 363 (2023) 507–524, https://doi.org/10.1016/j.jconrel.2023.10.002.

[5] J.D. McAllaster, M.S. Cohen, Role of the lymphatics in cancer metastasis and chemotherapy applications, Adv. Drug Deliv. Rev. 63 (2011) 867–875, https://doi.org/10.1016/j.addr.2011.05.014.

[6] K.G.M. Brown, C.E. Koh, Surgical management of recurrent colon cancer, J. Gastrointest. Oncol. 11 (2020) 513–525, https://doi.org/10.21037/jgo-2019-ccm-09.

[7] H. Petrowsky, R. Fritsch, M. Guckenberger, M.L. De Oliveira, P. Dutkowski, P.-A. Clavien, Modern therapeutic approaches for the treatment of malignant liver tumours, Nat. Rev. Gastroenterol. Hepatol. 17 (2020) 755–772, https://doi.org/10.1038/s41575-020-0314-8.

[8] J.U. Lim, C.D. Yeo, Update on adjuvant therapy in completely resected NSCLC PATIENTS, Thoracic Cancer 13 (2022) 277–283, https://doi.org/10.1111/1759-7714.14277.

[9] R.N. Amaria, A.M. Menzies, E.M. Burton, R.A. Scolyer, M.T. Tetzlaff, R. Antdbacka, C. Ariyan, R. Bassett, B. Carter, A. Daud, M. Faries, L.A. Fecher, K.T. Flaherty, J. E. Gershenwald, O. Hamid, A. Hong, J.M. Kirkwood, S. Lo, K. Margolin, J. Messina, M.A. Postow, H. Rizos, M.I. Ross, E.A. Rozeman, R.P.M. Saw, V. Sondak, R. J. Sullivan, J.M. Taube, J.F. Thompson, B.A. Van De Wiel, A.M. Eggermont, M. A. Davies, P.A. Ascierto, A.J. Spillane, A.C.J. Van Akkooi, J.A. Wargo, C.U. Blank, H.A. Tawbi, G.V. Long, M.C. Andrews, D.A. Berry, M.S. Block, G.M. Boland, K. B. Bollin, M.S. Carlino, R.D. Carvajal, J. Cohen, D. Davar, K.A. Delman, R. Dummer, M.D. Farwell, D.E. Fisher, A. Fusi, I.C. Glitza, T.D. De Gruijl, D.E. Gyorki, A. Hauschild, T.J. Hieken, J. Larkin, D.H. Lawson, C. Lebbe, J.E. Lee, M.C. Lowe, J. J. Luke, G.A. McArthur, D.F. McDermott, J.L. McQuade, T.C. Mitchell, T. M. Petrella, P.A. Prieto, I. Puzanov, C. Robert, A.K. Salama, S. Sandhu, D. Schadendorf, A.N. Shoushtari, J.A. Sosman, S.M. Swetter, K.K. Tanabe, S. Turajlic, D.S. Tyler, S.E. Woodman, F.C. Wright, J.S. Zager, Neoadjuvant systemic therapy in melanoma: recommendations of the International Neoadjuvant Melanoma Consortium, Lancet Oncol. 20 (2019) e378–e389, https://doi.org/10.1016/S1470-2045(19)30332-8.

[10] M.T. Manzari, Y. Shamay, H. Kiguchi, N. Rosen, M. Scaltriti, D.A. Heller, Targeted drug delivery strategies for precision medicines, Nat. Rev. Mater. 6 (2021) 351–370, https://doi.org/10.1038/s41578-020-00269-6.

[11] Z. Zhao, A. Ukidve, J. Kim, S. Mitragotri, Targeting strategies for tissue-specific drug delivery, Cell 181 (2020) 151–167, https://doi.org/10.1016/j.cell.2020.02.001.

[12] M. Yousef, D. Silva, N. Bou Chacra, N. Davies, R. Löbenberg, The Lymphatic System: A Sometimes-Forgotten Compartment in Pharmaceutical Sciences, J. Pharm.Sci. 24 (2021) 533–547, https://doi.org/10.18433/jpps32222.

[13] A.D. Permana, F. Nainu, K. Moffatt, E. Larrañeta, R.F. Donnelly, Recent Advances in Combination of Microneedles and Nanomedicines for Lymphatic Targeted Drug Delivery, WIREs Nanomed Nanobiotechnol 13, 2021, https://doi.org/10.1002/wnan.1690.

[14] H. Jiang, Q. Wang, X. Sun, Lymph node targeting strategies to improve vaccination efficacy, J. Control. Release 267 (2017) 47–56, https://doi.org/10.1016/j.jconrel.2017.08.009.

[15] X. Peng, J. Wang, F. Zhou, Q. Liu, Z. Zhang, Nanoparticle-based approaches to target the lymphatic system for antitumor treatment, Cell. Mol. Life Sci. 78 (2021) 5139–5161, https://doi.org/10.1007/s00018-021-03842-6.

[16] S. Babity, A.K. Polomska, F. Couture, M. Bonmarin, D. Fehr, M. Detmar, D. Brambilla, Rational design of a fluorescent microneedle tattoo for minimally invasive monitoring of lymphatic function, J. Control. Release 327 (2020) 350–359, https://doi.org/10.1016/j.jconrel.2020.08.017.

[17] N.L. Trevaskis, L.M. Kaminskas, C.J.H. Porter, From sewer to saviour — targeting the lymphatic system to promote drug exposure and activity, Nat. Rev. Drug Discov. 14 (2015) 781–803, https://doi.org/10.1038/nrd4608.

[18] T.C. De Oliveira, M.E.V. Tavares, J.L. Soares-Sobrinho, L.L. Chaves, The role of nanocarriers for transdermal application targeted to lymphatic drug delivery: opportunities and challenges, J.Drug Delivery Sci. and Technol. 68 (2022) 103110, https://doi.org/10.1016/j.jddst.2022.103110.

[19] M. Hegde, N. Naliyadhara, J. Unnikrishnan, M.S. Alqahtani, M. Abbas, S. Girisa, G. Sethi, A.B. Kunnumakkara, Nanoparticles in the diagnosis and treatment of cancer metastases: current and future perspectives, Cancer Lett. 556 (2023) 216066, https://doi.org/10.1016/j.canlet.2023.216066.

[20] A.H. Sabri, Y. Kim, M. Marlow, D.J. Scurr, J. Segal, A.K. Banga, L. Kagan, J.B. Lee, Intradermal and transdermal drug delivery using microneedles – fabrication, performance evaluation and application to lymphatic delivery, Adv. Drug Deliv. Rev. 153 (2020) 195–215, https://doi.org/10.1016/j.addr.2019.10.004.

[21] A. Obinu, E. Gavini, G. Rassu, M. Maestri, M.C. Bonferoni, P. Giunchedi, Lymph node metastases: importance of detection and treatment strategies, Expert Opin. Drug Deliv. 15 (2018) 459–467, https://doi.org/10.1080/17425247.2018.1446937.

[22] Y. Sakurai, A. Ohtani, Y. Nakayama, M. Gomi, T. Masuda, S. Ohtsuki, H. Tanaka, H. Akita, Logistics and distribution of small extracellular vesicles from the subcutaneous space to the lymphatic system, J. Control. Release 361 (2023) 77–86, https://doi.org/10.1016/j.jconrel.2023.07.043.

[23] S.A.T. Opatha, V. Titapiwatanakun, R. Chutoprapat, Transfersomes: a promising Nanoencapsulation technique for transdermal drug delivery, Pharmaceutics 12 (2020) 855, https://doi.org/10.3390/pharmaceutics12090855.

[24] G. Cevc, Transfersomes, Liposomes and Other Lipid Suspensions on the Skin: Permeation Enhancement, Vesicle Penetration, and Transdermal Drug Delivery, Crit. Rev. Ther. Drug Carrier Syst. 13 (1996) 257–388, https://doi.org/10.1615/CritRevTherDrugCarrierSyst.v13.i3-4.30.

[25] P. Oyarzún, E. Gallardo-Toledo, J. Morales, F. Arriagada, Transfersomes as alternative topical nanodosage forms for the treatment of skin disorders, Nanomedicine 16 (2021) 2465–2489, https://doi.org/10.2217/nnm-2021-0335.

[26] G.M.M. El Maghraby, A.C. Williams, B.W. Barry, Can drug-bearing liposomes penetrate intact skin? J. Pharm. Pharmacol. 58 (2010) 415–429, https://doi.org/10.1211/jpp.58.4.0001.

[27] H. Yang, X. Wu, Z. Zhou, X. Chen, M. Kong, Enhanced transdermal lymphatic delivery of doxorubicin via hyaluronic acid based transfersomes/microneedle complex for tumor metastasis therapy, Int. J. Biol. Macromol. 125 (2019) 9–16, https://doi.org/10.1016/j.ijbiomac.2018.11.230.

[28] M. Sharma, N. Mittapelly, V.T. Banala, S. Urandur, S. Gautam, D. Marwaha, N. Rai, N. Singh, A. Gupta, K. Mitra, P.R. Mishra, Amalgamated microneedle Array bearing Ribociclib-loaded Transfersomes eradicates breast Cancer *via* CD44 targeting, Biomacromolecules 23 (2022) 661–675, https://doi.org/10.1021/acs.biomac.1c01076.

[29] M. Kong, L. Hou, J. Wang, C. Feng, Y. Liu, X. Cheng, X. Chen, Enhanced transdermal lymphatic drug delivery of hyaluronic acid modified transfersomes for tumor metastasis therapy, Chem. Commun. 51 (2015) 1453–1456, https://doi.org/10.1039/C4CC08746A.

[30] X. Wu, Y. Li, X. Chen, Z. Zhou, J. Pang, X. Luo, M. Kong, A surface charge dependent enhanced Th1 antigen-specific immune response in lymph nodes by transfersome-based nanovaccine-loaded dissolving microneedle-assisted transdermal immunization, J. Mater. Chem. B 7 (2019) 4854–4866, https://doi.org/10.1039/C9TB00448C.

[31] Z. Zhou, J. Pang, X. Wu, W. Wu, X. Chen, M. Kong, Reverse immune suppressive microenvironment in tumor draining lymph nodes to enhance anti-PD1 immunotherapy via nanovaccine complexed microneedle, Nano Res. 13 (2020) 1509–1518, https://doi.org/10.1007/s12274-020-2737-5.

[32] A.J. Guillot, A.S. Cordeiro, R.F. Donnelly, M.C. Montesinos, T.M. Garrigues, A. Melero, Microneedle-based delivery: an overview of current applications and trends, Pharmaceutics 12 (2020) 569, https://doi.org/10.3390/pharmaceutics12060569.

[33] Z. Sartawi, C. Blackshields, W. Faisal, Dissolving microneedles: applications and growing therapeutic potential, J. Control. Release 348 (2022) 186–205, https://doi.org/10.1016/j.jconrel.2022.05.045.

[34] U. Detamornrat, E. McAlister, A.R.J. Hutton, E. Larrañeta, R.F. Donnelly, The role of 3D printing Technology in Microengineering of microneedles, Small 18 (2022) 2106392, https://doi.org/10.1002/smll.202106392.

[35] R. Jamaledin, C.K.Y. Yiu, E.N. Zare, L. Niu, R. Vecchione, G. Chen, Z. Gu, F.R. Tay, P. Makvandi, Advances in antimicrobial microneedle patches for combating infections, Adv. Mater. 32 (2020) 2002129, https://doi.org/10.1002/adma.202002129.

[36] A.H. Sabri, J. Ogilvie, K. Abdulhamid, V. Shpadaruk, J. McKenna, J. Segal, D. J. Scurr, M. Marlow, Expanding the applications of microneedles in dermatology, Eur. J. Pharm. Biopharm. 140 (2019) 121–140, https://doi.org/10.1016/j.ejpb.2019.05.001.

[37] S.C. Balmert, C.D. Carey, G.D. Falo, S.K. Sethi, G. Erdos, E. Korkmaz, L.D. Falo, Dissolving undercut microneedle arrays for multicomponent cutaneous vaccination, J. Control. Release 317 (2020) 336–346, https://doi.org/10.1016/j.jconrel.2019.11.023.

[38] S. Demartis, Q.K. Anjani, F. Volpe-Zanutto, A.J. Paredes, S.A. Jahan, L.K. Vora, R. F. Donnelly, E. Gavini, Trilayer Dissolving Polymeric Microneedle Array Loading Rose Bengal Transfersomes as a Novel Adjuvant in Early-Stage Cutaneous Melanoma Management, Int. J. Pharm. 627 (2022), https://doi.org/10.1016/j.ijpharm.2022.122217.

[39] S. Demartis, G. Rassu, S. Murgia, L. Casula, P. Giunchedi, E. Gavini, Improving dermal delivery of rose Bengal by deformable lipid Nanovesicles for topical treatment of melanoma, Mol. Pharm. 18 (2021) 4046–4057, https://doi.org/10.1021/acs.molpharmaceut.1c00468.

[40] S. Demartis, A. Obinu, E. Gavini, P. Giunchedi, G. Rassu, Nanotechnology-Based Rose Bengal: A Broad-Spectrum Biomedical Tool, Dyes and Pigments 188, 2021, https://doi.org/10.1016/j.dyepig.2021.109236.

[41] P. Toomey, K. Kodumudi, A. Weber, L. Kuhn, E. Moore, A.A. Sarnaik, S. Pilon-Thomas, Intralesional injection of rose Bengal induces a systemic tumor-specific immune response in murine models of melanoma and breast Cancer, PLoS One 8 (2013) e68561, https://doi.org/10.1371/journal.pone.0068561.

[42] S.B. Koevary, Selective toxicity of rose bengal to ovarian cancer cells in vitro, Int. J. Physiol. Pathophysiol. Pharmacol. 4 (2012) 99–107.

[43] J. Qin, N. Kunda, G. Qiao, J.F. Calata, K. Pardiwala, B.S. Prabhakar, A.V. Maker, Colon cancer cell treatment with rose bengal generates a protective immune response via immunogenic cell death, Cell Death Dis. 8 (2017) e2584, https://doi.org/10.1038/cddis.2016.473.

[44] A.V. Maker, B. Prabhakar, K. Pardiwala, The potential of Intralesional rose Bengal to stimulate T-cell mediated anti-tumor responses, J. Clin. Cell Immunol. 6 (2015) 343, https://doi.org/10.4172/2155-9899.1000343.

[45] C.D. Klaassen, Pharmacokinetics of rose bengal in the rat, rabbit, dog, and guinea pig, Toxicol. Appl. Pharmacol. 38 (1976) 85–100, https://doi.org/10.1016/0041-008X(76)90163-0.

[46] M. Wiener, D.L. Damian, J.F. Thompson, Systemic Phototoxicity following Intralesional rose Bengal for subcutaneous melanoma metastases, Dermatology 216 (2008) 361–362, https://doi.org/10.1159/000117707.

[47] Q.K. Anjani, S. Demartis, F. Volpe-Zanutto, H. Li, A.H.B. Sabri, E. Gavini, R. F. Donnelly, Fluorescence-coupled techniques for determining rose Bengal in dermatological formulations and their application to ex vivo skin deposition studies, Pharmaceutics 15 (2023) 408, https://doi.org/10.3390/pharmaceutics15020408.

[48] T. Waghule, V.K. Rapalli, G. Singhvi, S. Gorantla, A. Khosa, S.K. Dubey, R.N. Saha, Design of temozolomide-loaded proliposomes and lipid crystal nanoparticles with industrial feasible approaches: comparative assessment of drug loading, entrapment efficiency, and stability at plasma pH, J. Liposome Res. 31 (2021) 158–168, https://doi.org/10.1080/08982104.2020.1748648.

[49] N. Rezaei, F. Mehrnejad, Z. Vaezi, M. Sedghi, S.M. Asghari, H. Naderi-Manesh, Encapsulation of an endostatin peptide in liposomes: stability, release, and cytotoxicity study, Colloids Surf. B: Biointerfaces 185 (2020) 110552, https://doi.org/10.1016/j.colsurfb.2019.110552.

[50] N. Ding, Y. Wang, X. Wang, W. Chu, T. Yin, J. Gou, H. He, Y. Zhang, Y. Wang, X. Tang, Improving plasma stability and antitumor effect of gemcitabine via PEGylated liposome prepared by active drug loading, J.Drug Delivery Sci. and Technol. 57 (2020) 101538, https://doi.org/10.1016/j.jddst.2020.101538.

[51] M.T.A. Abbate, I.K. Ramöller, A.H. Sabri, A.J. Paredes, A.J. Hutton, P.E. McKenna, K. Peng, J.A. Hollett, H.O. McCarthy, R.F. Donnelly, Formulation of antiretroviral nanocrystals and development into a microneedle delivery system for potential treatment of HIV-associated neurocognitive disorder (HAND), Int. J. Pharm. 640 (2023) 123005, https://doi.org/10.1016/j.ijpharm.2023.123005.

[52] J.F. Thompson, P. Hersey, E. Wachter, Chemoablation of metastatic melanoma using intralesional rose Bengal, Melanoma Res. 18 (2008) 405, https://doi.org/10.1097/CMR.0b013e32831328c7.

[53] Y.A. Naser, I.A. Tekko, L.K. Vora, K. Peng, Q.K. Anjani, B. Greer, C. Elliott, H. O. McCarthy, R.F. Donnelly, Hydrogel-forming microarray patches with solid dispersion reservoirs for transdermal long-acting microdepot delivery of a hydrophobic drug, J. Control. Release 356 (2023) 416–433, https://doi.org/10.1016/j.jconrel.2023.03.003.

[54] Y. Zhang, M. Huo, J. Zhou, S. Xie, PKSolver: an add-in program for pharmacokinetic and pharmacodynamic data analysis in Microsoft excel, Comput. Methods Prog. Biomed. 99 (2010) 306–314, https://doi.org/10.1016/j.cmpb.2010.01.007.

[55] K. Peng, L.K. Vora, I.A. Tekko, A.D. Permana, J. Domínguez-Robles, D. Ramadon, P. Chambers, H.O. McCarthy, E. Larrañeta, R.F. Donnelly, Dissolving microneedle patches loaded with amphotericin B microparticles for localised and sustained intradermal delivery: potential for enhanced treatment of cutaneous fungal infections, J. Control. Release 339 (2021) 361–380, https://doi.org/10.1016/j.jconrel.2021.10.001.

[56] GraphPad Prism 10 Statistics Guide - STATISTICS WITH PRISM 10. https://www.graphpad.com/guides/prism/latest/statistics/stat_—_statistics_with_prism_6_–.htm , 2024 (accessed August 22, 2023).

[57] K. Iwuozor, Properties and Uses of Colloids: A Review, Colloid and Surface Science 4 (2019) 24–28. doi:10.11648/j.css.20190402.12.

[58] Y. Jin, D. Liu, Z. Lu, L. Yang, J. Chen, X. Zhou, Z. Qiu, Y. Jin, Preparation and Evaluation of Liposomes and Niosomes Containing Total Ginsenosides for Anti-Photoaging Therapy, Frontiers in Bioengineering and Biotechnology 10. https://www.frontiersin.org/articles/10.3389/fbioe.2022.874827, 2022 (accessed July 27, 2023).

[59] C.-C. Chang, Y.-T. Yang, J.-C. Yang, H.-D. Wu, T. Tsai, Absorption and emission spectral shifts of rose bengal associated with DMPC liposomes, Dyes Pigments 79 (2008) 170–175, https://doi.org/10.1016/j.dyepig.2008.02.003.

[60] F. Forouz, M. Dabbaghi, S. Namjoshi, Y. Mohammed, J.E. Grice, Development of an oil-in-water self-emulsifying microemulsion for cutaneous delivery of rose Bengal: investigation of anti-melanoma properties, Pharmaceutics 12 (2020) 947, https://doi.org/10.3390/pharmaceutics12100947.

[61] B. Slivinschi, F. Manai, C. Martinelli, F. Carriero, C. D'Amato, M. Massarotti, G. Bresciani, C. Casali, G. Milanesi, L. Artal, L. Zanoletti, F. Milella, D. Arfini,

A. Azzalin, S. Demartis, E. Gavini, S. Comincini, Enhanced Delivery of Rose Bengal by Amino Acids Starvation and Exosomes Inhibition in Human Astrocytoma Cells to Potentiate Anticancer Photodynamic Therapy Effects, Cells 11, 2022, https://doi.org/10.3390/cells11162502.

[62] K. Sztandera, M. Gorzkiewicz, E.A. Zizzi, N. Dybczak, L. Poltorak, M.A. Deriu, B. Klajnert-Maculewicz, Cellular uptake of rose bengal is mediated by OATP1B1/1B3 transporters, Bioelectrochemistry 152 (2023) 108449, https://doi.org/10.1016/j.bioelechem.2023.108449.

[63] P. Nakhaei, R. Margiana, D.O. Bokov, W.K. Abdelbasset, M.A. Jadidi Kouhbanani, R.S. Varma, F. Marofi, M. Jarahian, N. Beheshtkhoo, Liposomes: Structure, Biomedical Applications, and Stability Parameters with Emphasis on Cholesterol, Front. Bioengineering and Biotechnol. 9 (2021). https://www.frontiersin.org/articles/10.3389/fbioe.2021.705886. (Accessed 1 August 2023).

[64] E. Hugo, E. Abuin, E. Lissi, E. Alarcón, A.M. Edwards, Effect of temperature on the photobehavior of rose Bengal associated with dipalmitoylphosphatidyl choline liposomes, JOL 131 (2011) 2468–2472, https://doi.org/10.1016/j.jlumin.2011.06.021.

[65] B. Sheikholeslami, N.W. Lam, K. Dua, M. Haghi, Exploring the impact of physicochemical properties of liposomal formulations on their in vivo fate, Life Sci. 300 (2022) 120574, https://doi.org/10.1016/j.lfs.2022.120574.

[66] E. Panzarini, V. Inguscio, L. Dini, Overview of cell death mechanisms induced by rose Bengal acetate-photodynamic therapy, International J. Photoenergy 2011 (2011) 1–11, https://doi.org/10.1155/2011/713726.

[67] S. Demartis, G. Rassu, V. Mazzarello, E. Larrañeta, A. Hutton, R.F. Donnelly, A. Dalpiaz, M. Roldo, A.J. Guillot, A. Melero, P. Giunchedi, E. Gavini, Delivering hydrosoluble compounds through the skin: what are the chances? Int. J. Pharm. 123457 (2023) https://doi.org/10.1016/j.ijpharm.2023.123457.

[68] C.A. Téllez-Soto, M.G. Pereira Silva, L. dos Santos, T. de O. Mendes, P. Singh, S. A. Fortes, P. Favero, A.A. Martin, In vivo determination of dermal water content in chronological skin aging by confocal Raman spectroscopy, Vib. Spectrosc. 112 (2021) 103196, https://doi.org/10.1016/j.vibspec.2020.103196.

[69] H.M. Redhead, S.S. Davis, L. Illum, Drug delivery in poly(lactide-co-glycolide) nanoparticles surface modified with poloxamer 407 and poloxamine 908: in vitro characterisation and in vivo evaluation, J. Control. Release 70 (2001) 353–363, https://doi.org/10.1016/S0168-3659(00)00367-9.

[70] Z. Yang, J. Liu, J. Gao, S. Chen, G. Huang, Chitosan coated vancomycin hydrochloride liposomes: characterizations and evaluation, Int. J. Pharm. 495 (2015) 508–515, https://doi.org/10.1016/j.ijpharm.2015.08.085.

[71] A.J. Guillot, M. Martínez-Navarrete, T.M. Garrigues, A. Melero, Skin drug delivery using lipid vesicles: a starting guideline for their development, J. Control. Release 355 (2023) 624–654, https://doi.org/10.1016/j.jconrel.2023.02.006.

[72] D. Han, C. Li, S. Araimdeh, V. Sree, E. Rahimi, A. Buganza Tepole, A.M. Ardekani, Lymphatic uptake of biotherapeutics through a 3D hybrid discrete-continuum vessel network in the skin tissue, J. Control. Release 354 (2023) 869–888, https://doi.org/10.1016/j.jconrel.2022.12.045.

[73] I.L. Ramöller, F. Volpe-Zanutto, L.K. Vora, M.T.A. Abbate, A.R.J. Hutton, P. E. McKenna, K. Peng, I.A. Tekko, A. Sabri, E. McAlister, H.O. McCarthy, A. J. Paredes, R.F. Donnelly, Intradermal delivery of the antiretroviral drugs cabotegravir and rilpivirine by dissolving microarray patches: Investigation of lymphatic uptake, J. Control. Release 366 (2024) 548–566, https://doi.org/10.1016/j.jconrel.2024.01.010.

[74] Y. Sakurai, K. Yoshikawa, K. Arai, A. Kazaoka, S. Aoki, K. Ito, Y. Nakai, K. Tange, T. Furihata, H. Tanaka, H. Akita, siRNA delivery to lymphatic endothelial cells via ApoE-mediated uptake by lipid nanoparticles, J. Control. Release 353 (2023) 125–133, https://doi.org/10.1016/j.jconrel.2022.11.036.